ACS APPLIED MATERIALS & INTERFACES

Research Article

www.acsami.org

Redox Tuning and Species Distribution in Maya Blue-Type Materials: A Reassessment

Antonio Doménech-Carbó,*[,†] Francisco Manuel Valle-Algarra,[†] María Teresa Doménech-Carbó,[‡] Marcelo E. Domine,[§] Laura Osete-Cortina,[‡] and José Vicente Gimeno-Adelantado[†]

[†]Departament de Química Analítica, Universitat de València, Dr. Moliner, 50, 46100 Burjassot València, Spain

[‡]Institut de Restauració del Patrimoni, Universitat Politècnica de València, Camí de Vera s/n, 46022 València, Spain

[§]Instituto de Tecnología Química (ITQ), Universitat Politècnica de València−CSIC, Avda. Los Naranjos s/n, 46022 Valencia, Spain

Supporting Information

ABSTRACT: Maya Blue-type specimens prepared from indigo (1 wt %) plus kaolinite, montmorillonite, palygorskite, sepiolite, and silicalite are studied. Liquid chromatography with diode array detection, ultra-performance liquid chromatography coupled with mass spectrometry, and pyrolysis-silylation gas chromatography−mass spectrometry analyses of the extracts from these specimens combined with spectral and solid-state voltammetry, electrochemical impedance spectroscopy, and scanning electrochemical microscopy techniques provide evidence for the presence of a significant amount of dehydroindigo and isatin accompanying indigo and other minority organic compounds in all samples. Solid-state electrochemistry data permits the estimation of indigo loading in archeological Maya Blue, which is in the range of 0.2 to 1.5 wt %. These results support a view of 'genuine' Maya Blue-type materials as complex polyfunctional organic−inorganic hybrids.

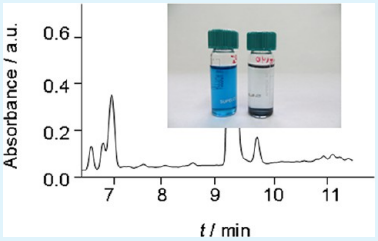

KEYWORDS: *Maya Blue, dehydroindigo, indigo, isatin, palygorskite, sepiolite, silicalite, kaolinite, montmorillonite*

I. INTRODUCTION

There is considerable interest in the preparation of organic−inorganic hybrid materials resulting from the attachment of dyes to aluminosilicate supports because of their combination of chemical stability and pigmenting properties.[1−3] Ultimately, such materials can be considered to be a legacy from Maya Blue, which is an ancient nanostructured material[4] discovered by Merwin in 1931.[5] Maya Blue, which is widely used in wall paintings, pottery, and sculptures by the Mayas and other ancient Mesoamerican cultures in pre-Columbian times, has received attention because of its unusual durability and characteristic hue. The pigment, whose hybrid organic−inorganic composition was first proposed by Sheppard in 1962,[6] results from the attachment of indigo (or indigotin), 3*H*-indol-3-one-2-(1,3-dihydro-3-oxo-2*H*-indol-2-ylidene)-1,2-dihydro-(2*E*), a blue dye extracted in Mesoamerica from leaves of *añil* or *xiuquitlitl* (*Indigofera suffruticosa* and other species), to palygorskite (or attapulgite), a fibrous phyllosilicate clay of ideal composition $Si_8(Mg_2Al_2)O_{20}(OH)_2(H_2O)_4{\cdot}4H_2O$. In spite of intensive research, there is controversy regarding the nature of the indigo−palygorskite association, the location of the dye molecules on the clay support, and the origin of the peculiar color of the pigment and its variability.[7−24]

In fact, the preparation of the historical pigment, because of the absence of historical sources describing it, remains unknown.[25] Different preparation recipes involving vat dyeing and dry indigo plus clay crushing are available.[26,27] In general, the dry preparation of Maya Blue-type materials via grinding a mixture of the solid dye and the clay followed by a subsequent heating at temperatures between 100 and 200 °C is used.[11−24] This methodology has been recently applied to prepare different indigo-based hybrid materials, namely, indigo-palygorskite (IN@PL),[28,29] indigo-sepiolite (IN@SP),[30−36] and indigo-zeolites[37,38] as well as hybrids from dyes such as alizarin,[39] methyl red,[40] and sepiolite. Sepiolite is a fibrous magnesium silicate (ideal formula of $Mg_4Si_6O_{15}(OH)_2{\cdot}6H_2O$), and its channels have larger dimensions than those of palygorskite. Kaolinite ($Al_2Si_2O_5(OH)_4$) is a layered silicate with one tetrahedral sheet linked through oxygen atoms to one sheet of alumina octahedral, whereas montmorillonite ($(Na,Ca)_{0.33}(Al,Mg)_2(Si_4O_{10})(OH)_2{\cdot}nH_2O$) has two tetrahedral sheets sandwiching a central octahedral sheet. To complete the scope of usual silicate clays employed in Maya Blue studies, silicalite, an MFI-type zeolite that can be described as a 3D porous silicate with two interconnected tubular channel systems involving sinusoidal channels of 5.5 × 5.1 Å in size, is used and straight channels of 5.5 × 5.6 Å in size. This zeolite support provides trap possibilities different from those of palygorskite and sepiolite, which possess channels of 6.4 × 3.7 and 10.3 × 3.7 Å in size, respectively.

In previous reports, we used the voltammetry of microparticles, a solid-state electrochemical methodology developed by Scholz et al. that provides analytical information on sparingly soluble solids,[41−43] combined with infrared (ATR−FTIR) and

Received: June 6, 2013
Accepted: July 26, 2013
Published: July 26, 2013

Table 1. ^{1}H and ^{13}C NMR and MS Data for the Identification of Indigo, Dehydroindigo, and Isatin in the DMSO Extracts of IN@MT_{150}

compound	^{1}H NMR	^{13}C NMR	$[M + H]^{+}$ (m/z)
indigo	7.04−7.63 (m, 8H), 10.7 (N−H)	191.1 (C-3), 153.5 (C-2), 137.8, 125.1, 124.1, 122.3, 120.5, 113.3	263.0821
dehydroindigo	7.76−7.64 (m, 8H)	189.48 (C-3), 159.52 (C-2), 155.24 (C-3a), 139.12 (C-7a), 136.81 (C-6), 130.36 (C-4), 125.04 (C-5), 124.40 (C-7)	261.0582
isatin	4.32 (N−H), 6.86 (d), 7.01 (t), 7.47 (d), 7.55 (t)	184.5 (C-3), 159.5 (C-2), 151.0 (C-7a), 138.8 (C-6), 124.5 (C-4), 123.3 (C-5), 118.0 (C-3a), 112.3 (C-7)	148.0393

visible spectroscopies and electron (SEM/EDX, TEM) and atomic force microscopy (AFM) techniques to propose that dehydroindigo, which is one oxidized form of indigo, accompanies this dye in the historical pigment. Thus, the variation in the dehydroindigo/indigo ratio would determine the variable greenish-blue hue of the pigment observed in archeological samples and synthetic specimens.[44−47] As a result, we advocated a view of MB as a polyfunctional hybrid inorganic−organic material where different dye molecules could be located in different clay sites, defining different topological redox isomers,[48,49] which is in line with recently reviewed formulations of the chemistry and electrochemistry of microporous materials.[50]

However, the examination of literature data reveals that these materials are predominantly seen as constituted by a unique organic component. Sánchez del Río et al.,[23,28] Martinetto et al.,[29,32] Chryssikos et al.,[24] and Giulieri et al.,[34−36] who used dry preparative methods and indigo loadings between 1 and 20%, did not find dye molecules other than indigo in their indigo plus support (IN@support) specimens. The same conclusion is reported by Lima et al.[27] using different wet vat-dyeing methods. In this regard, it should be noted that the indigo loading and preparation method play a crucial role in the properties of the resulting materials. In fact, most of the prepared materials involve indigo loadings larger than the theoretical maximum channel occupation in palygorskite (ca. 4 wt %)[51] as well as the value that is considered typical for historical Maya Blue (ca. 1 wt %), as recognized by Mondelli et al.,[28] thus making the detection of minority components difficult.

The purpose of the current report is to provide a set of data on synthetic Maya Blue-type specimens focused on two aspects: (a) the existence of redox tuning in IN@support materials and (b) the differences in the distribution of the dye component in the crystals of the inorganic support. Three types of supports were compared: (i) phyllosilicate clays containing channels theoretically able to trap indigo molecules (palygorskite and sepiolite), (ii) laminar clays with no channels for dye insertion (kaolinite and montmorillonite), and (iii) a MFI zeolite where indigo could in principle be encapsulated within cages experiencing constraints different from those of the above phyllosilicate clays (silicalite). The problem of the historical quantitative composition of Maya Blue will be treated here using solid-state electrochemical data. In agreement with previous results on IN@PL specimens,[52] the essential idea is that dehydroindigo (and other minority organic components) is a ubiquitous component of genuine Maya Blue-type materials prepared with historical indigo loadings (1 wt %). We advocate the view that genuine, in the historical meaning, Maya Blue-type materials are characterized by just their multicomponent and polyfunctional nature so that most of the prepared IN@support materials could not be considered Mayan materials.

Here, analytical data on synthetic specimens, prepared from indigo (1 wt %) with kaolinite, montmorillonite, palygorskite, sepiolite, and silicalite using the conventional dry procedure, are provided. The specimens were characterized by FTIR spectroscopy, UV−vis spectrophotometry, and solid-state electrochemistry. The separation and identification of organic components in the extracts from such specimens was performed via liquid chromatography with diode array detection (LC−DAD), ultra-performance liquid chromatography coupled with mass spectrometry (UPLC−MS), and pyrolysis-silylation gas chromatography−mass spectrometry (Py-GC−MS). The speciation and in depth species distribution were analyzed using chronoamperometry (CA), electrochemical impedance spectroscopy (EIS), and scanning electrochemical microscopy (SECM) techniques. EIS is a technique widely used for characterizing materials and their surface properties[50] because of its ability to provide information on phenomena occurring on considerably different time scales. SECM is technique providing an electrochemical topography image of surfaces, on the nanoscopic scale,[53] which has been applied for the micropatterning of metal oxide thin films[54] or the immobilization of organic molecules into self-assembled monolayers.[55]

II. EXPERIMENTAL SECTION

II.1. Reagents, Reference Products, and MB-Like Specimen Preparation. Methanol, dimethyl sulfoxide (Carlo Erba), and hexamethyldisilazane (HMDS) (Sigma-Aldrich) (purity 99%) were used in chromatographic experiments. Indigo (Fluka), isatin, (Aldrich), and indirubin (RG Chromadex) were used as reference dyes. Dehydroindigo was prepared following reported procedures[56,57] and characterized by UV−vis spectroscopy, ^{1}H and ^{13}C nuclear magnetic resonance spectroscopy, and MS. The obtained spectra agreed entirely with those in the literature[57] (Table 1). Palygorskite (PL), collected from the Sak lu'um classical site in Yucatan,[43−47] was used. Kaolinite (KA), montmorillonite (MT), and sepiolite (SP) were obtained from the mineral repository of the University of Valencia and characterized by their ATR−FTIR spectra and X-ray diffractograms (XRD). Silicalite was prepared as described by Yang and Lin[58] (BET surface area of 425 m^2/g, nominal Si/Al ratio ∞). Maya Blue-type specimens were prepared by finely grinding the inorganic support and mixing it with indigo (1.0 wt %) in an agate mortar and pestle for 60 min. The resulting specimens were separated in different portions and subjected to heating at temperatures, *T*, between 100 and 180 °C for 24 h (labeled as IN@$support_t$). Subsequently, the specimens were repeatedly rinsed with DMSO and acetone to remove the indigo that remained unattached to the clay. These conditions were selected within a suitable temperature interval owing to the fact that a previous kinetic study indicated the reaction completion for forming the indigo/dehydroindigo/palygorskite complex.[59] Blank experiments were also performed with specimens prepared at 25 °C with no subsequent heating (IN@PL_{25}, IN@KA_{25}, IN@MT_{25}, IN@SI_{25}, and IN@SP_{25}) and with indigo powder subjected to heating at temperatures between 100 and 180 °C (IN_t).

II.2. Instrumentation and Procedures. Aliquots of 0.100 g of the different IN@$support_t$ samples were subjected to extraction with 1 mL

of DMSO, 90:10 (v/v), H_2O/MeOH, and MeOH/DMSO, 50:50 (v/v), mixtures in closed vials. Prior to the extraction, the suspensions were maintained for 24 h under magnetic stirring. The resulting extracts were compared with those obtained independently from solutions of indigo, isatin, and dehydroindigo in the same solvents.

The extracts were injected into LC−DAD equipment consisting of an Agilent 1200 Series HPLC system equipped with a UV−vis diode array detector set at 286 nm (Agilent Technologies, Palo Alto, CA). The column was an Agilent Zorbax XDB C18 150 × 4.6 mm^2 (5 μm particle size) (Agilent) preceded by an Agilent Zorbax guard cartridge. Signals were processed by Agilent ChemStation software version 10.02 [1757]. The analysis was performed in the gradient mode. The mobile phase was a mixture of two solvents (solvent A was water−0.1% formic acid and solvent B was acetonitrile). Gradient conditions were initiated by holding the mobile phase composition for 0.1 min with 7% solvent B, after which it was changed linearly to 75% solvent B for 12 min. The composition was then changed to 98% solvent B in 3 min and maintained for 4.5 min as a cleaning step to improve the results. After cleaning, the eluent composition was returned to the initial 7% solvent B. The flow rate of the mobile phase was 1.2 mL/min, and the injection volume was 10 μL. The column oven was operated at 35 °C.

UPLC−MS analyses of the extracts obtained from samples from the different reference materials and specimens were performed with an ACQUITY UPLC system (Waters Corp.) with a conditioned autosampler at 4 °C. Liquid samples were prepared by diluting 0.1 mL of the extracts in 1.0 mL of acetonitrile. Typically, 10 μL of the prepared sample was injected into the UPLC system equipped with Phenomenex Kinetex XB-C18 column (100 × 4.6 mm^2 i.d. and 2.6 μm particle size). The column temperature was maintained at 40 °C. The mobile phase, pumped at 1.0 mL/min, consisted of 0.1% formic acid in water (A) and acetonitrile (B). The gradient applied was 7% B isocratic at 0.1 min, 75% B (linear) at 12 min, 98% B (linear) at 15 min, 98% B isocratic at 19.5 min, 7% B (linear) at 20.5 min, and 7% B isocratic until 25 min. The separated components of the sample mixture were detected with a Waters ACQUITY XevoQToF Spectrometer (Waters Corp.) connected to the UPLC system via an electro-spray ionization (ESI) interface. The ESI source was operated in positive ionization mode with the capillary voltage at 1.5 kV. The temperature of the source and desolvation was set at 100 and 400 °C, respectively. The cone and desolvation gas flows were 100 and 800 L/h, respectively. All data collected in Centroid mode were acquired using Masslynx software (Waters Corp.). Leucine-enkephalin was used as the lock mass, generating an $[M + H]^+$ ion (m/z = 556.2771) at a concentration of 2 ng/mL and flow rate of 50 μL/min to ensure accuracy during the MS analysis.

Py-GC−MS experiments were carried out with an integrated system composed of a CDS Pyroprobe 1000 heated filament pyrolyser (Analytical Inc., New York) and an Agilent 6890N (Agilent Technologies, Palo Alto, CA) gas chromatograph coupled to an Agilent 5973N mass spectrometer (Agilent Technologies) equipped with a pyrolysis injection system. A capillary column, HP-5MS (5% phenyl−95% methylpolysiloxane, 30 m, 0.25 mm i.d. and 0.25 μm film thickness; Agilent Technologies), was used to provide the adequate separation of the components. Pyrolysis was performed at 600 °C for 10 s using a precalibrated Pt coil-type pyrolyzer (CDS pyroprobe). The pyrolyser interface and the inlet were set at 250 °C. The samples were injected in split mode (split ratio 1:40). The chromatographic conditions were as follows: initial temperature of 50 °C held for 10 min and then increased at 5 °C min^{-1} up to 300 °C held for 8 min. The helium gas flow was set at 1.5 mL/min. The inlet pressure of the carrier gas was 89.1 kPa. The electronic pressure control was set to constant flow mode with vacuum compensation. Ions were generated by electron ionization (70 eV). The mass spectrometer was scanned from m/z 20 to m/z 800, with a cycle time of 1 s. Agilent Chemstation software G1701CA MSD was used for the GC−MS control, peak integration, and mass spectra evaluation. The tuning of the mass spectrometer was checked using perfluorotributylamine. EI mass spectra were acquired by total ion monitoring mode. The temperatures of the interface and the source were 280 and 150 °C, respectively. The Wiley Library of Mass Spectra and NIST were used for identifying the compounds. The samples were placed in a micro quartz pyrolysis tube, and two small portions of quartz wool were introduced in both sides of the quartz tube to avoid undesirable displacements of the sample, after which 5−10 μL of HMDS were added. Afterward, the sample was placed in the pyrolysis coil and introduced in the pyrolysis interface. At ca. 1 μg of solid sample, each reference material and specimen were introduced in a quartz tube with a small plug of quartz wool, with 1 μL of HMDS added afterward.

Voltammetry of microparticles experiments were performed with sample-modified paraffin-impregnated graphite electrodes (PIGEs) using a CH I660 potentiostat. A standard three-electrode arrangement was used with a platinum auxiliary electrode and a saturated calomel reference electrode (SCE) in a cell at 298 K. Experiments in aqueous media were performed with 0.25 M acetic acid/sodium acetate solutions at pH 4.75. For modified electrode preparation, ca. 0.5 mg of the samples were thoroughly powdered in an agate mortar and pestle and extended, forming a spot of finely distributed material. The lower end of the graphite electrode was pressed over that spot of sample to obtain a sample-modified surface. SECM experiments were performed on deposits of the IN@support materials on a graphite plate acting as a substrate electrode in contact with 5.0 mM $K_4Fe(CN)_6$ solution in 0.25 M HAc/NaAc (pH 4.75). Experiments were performed with CH 920c equipment using a microdisk platinum electrode tip (CH 49, diameter 20 μm) and a Pt substrate electrode. The bipotentiostat mode was used to apply potentials to the tip (E_T) and the electrode substrate (E_S). EIS measurements were performed at graphite electrodes covered by a deposit of IN@support specimens in the 0.01 to 100 000 Hz frequency range, with an amplitude of 10 mV upon application of different potentials using a 2.5 mM $K_4Fe(CN)_6$ + 2.5 mM $K_3Fe(CN)_6$ solution in 0.25 M HAc/NaAc (pH 4.75) aqueous buffer as a redox probe. ^1H and ^{13}C NMR measurements were acquired with a Bruker Advance 400 spectrometer operating at 399.91 MHz in deuterated DMSO. Transmission electron microscopy (TEM) was carried out with a JEM-1010 Jeol with Megaview III digital camera. A soft imaging system was used operating at 100 kV. MB samples were prepared by grinding a few micrograms of the samples in an agate mortar and dispersing them with an ultrasonic bath in ethanol. A drop of the dispersion was poured on TEM grids pretreated with a polymer film layer with holes to improve the quality of the images.

III. RESULTS AND DISCUSSION

III.1. TEM Examination of IN@support Specimens. Upon heating above 100 °C, all IN@support specimens, initially light blue, appeared as a turquoise-blue powder, as can be seen in Figure 1 in which photographic images of samples IN@SI_{140}, IN@SP_{140}, and IN@KA_{140} are shown. TEM examination of the specimens was performed to detect the possible features associated with dye attachment and to test the possible differences in the crystal texture occurring upon heating above 100 °C. No significant differences were found between the TEM images of the IN@SI_{25} and IN@SI_t samples and those of the silicalite crystals as well as between the IN@MT_{25} and IN@MT_t samples and montmorillonite (Supporting Information). In contrast, TEM images of IN@KA_{25} differed from those of IN@KA_{140}, as can be seen in Figure 2a,b. Pseudohexagonal kaolinite crystals,[60] after crushing with indigo (IN@KA_{25}), exhibited a series of irregular surface spots. The dehydration of kaolinite involves the structural disordering of laminar crystals and the formation of molecular dense aggregates,[61] whereas dehydroxylation occurs at temperatures above 400 °C,[62] so the observed spots are attributable to aggregates of indigo localized on the external surface of the crystals. After thermal treatment, a more regular spot distribution was observed, suggesting that upon heating indigo aggregates in the clay surface can experience some kind of chemical reaction resulting in changes in their distribution and

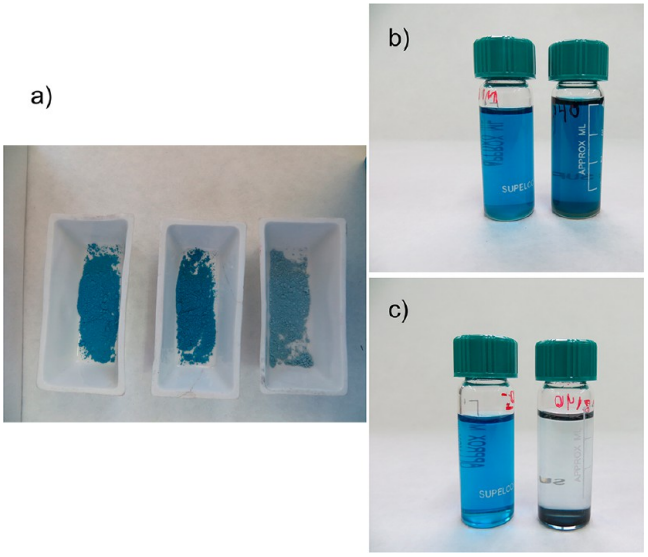

Figure 1. Photographic images of (a) samples IN@SI_{140} (left), IN@SP_{140}, and IN@KA_{140} (right); (b) samples IN@MT_{25} (left) and IN@MT_{150} (right) after extraction experiments; and (c) samples IN@SI_{25} (left) and IN@SI_{150} (right) after extraction experiments.

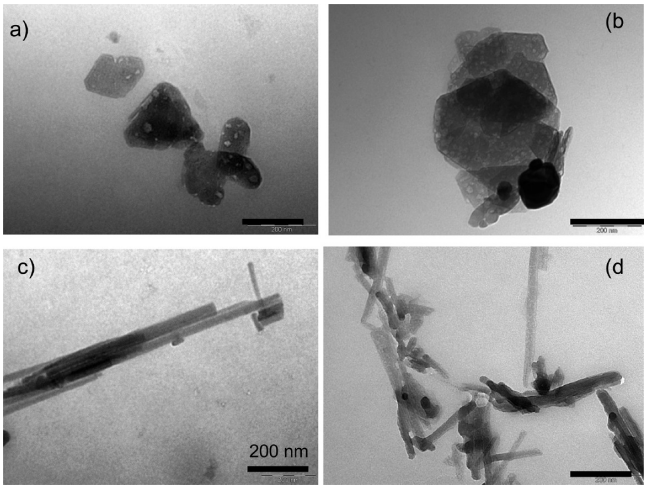

Figure 2. TEM images of specimens (a) IN@KA_{25}, (b) IN@KA_{140}, (c) IN@SP_{25}, and (d) IN@SP_{140}.

morphology. It is pertinent to note that in the case of laminar clays the attachment of indigo molecules may occur not only via adsorption to the flat side of the laminas but also via intercalation into the interlayer space between them, as described in the case of iron oxide particles associated with montmorillonite.[63]

In the case of the phyllosilicate clays, palygorskite and sepiolite, aggregates of acicular crystals of 0.5−1 μm in size having fine fiber structures with thicknesses from 300 to 600 Å were observed for the pristine clays[64] as well as the IN@SP_{25} and IN@PL_{25} specimens. In heated specimens, however, the crystals showed a more or less corrugated texture. As already described,[44−49] this feature, which often involves pore formation, can be associated to the evacuation of zeolitic water. In fact, pore formation in crystals associated with fast water evacuation has been reported for different minerals such as goethite.[65]

III.2. Extraction Experiments. Figure 1b compares the images of the DMSO extracts from IN@MT_{25} and IN@MT_{150}. In both cases, the supernatant solution is intensely blue, whereas the remaining solid becomes white (IN@MT_{25}) or light greenish-white (IN@MT_{150}). A similar behavior was obtained for IN@KA_t specimens. The above extraction behavior contrasts with that observed for MFI zeolite. As shown in Figure 1c for silicalite specimens, the IN@SI_{25} sample produces an intense blue extract accompanying a white solid; however, the IN@SI_{150} specimen yields an almost colorless DMSO extract over a blue-greenish solid material. This behavior is essentially identical to that obtained for the sepiolite and palygorskite samples. The extraction experiments can be summarized as follows: (i) in the case of the laminar clays, kaolinite and montmorillonite, the dye remains externally adsorbed and almost all is removed upon extraction for both unheated and heated specimens and (ii) nonheated specimens of microporous supports behave similarly, but specimens treated above 100 °C retain significant amounts of indigo (and other dyes, vide infra), so that after extraction the solid material maintain a blue-greenish coloration, whereas the extract is almost colorless.

These results can be rationalized by considering the diverse clay structures and assuming that (i) laminar clays can adsorb indigo (accompanied by aggregates of microcrystalline indigo), but this can be entirely or almost entirely removed by a conventional extraction with organic solvents regardless of the application of a previous thermal treatment to the samples and (ii) nonheated specimens prepared from microporous supports able to trap indigo molecules display a similar behavior, but heated specimens retain significant amounts of dye that is nonremovable in extraction experiments. This means that the thermal process is decisive for preparing protected materials.

LC−DAD and UPLC−MS of DMSO extracts from nonheated IN@$support_{25}$ specimens indicate the presence of indigo as a majority component accompanied by minor amounts of isatin, as can be seen in Figure 3 for IN@KA_{25}. LC−DAD and UPLC−MS of DMSO extracts from thermally treated specimens confirmed the presence of dehydroindigo, as

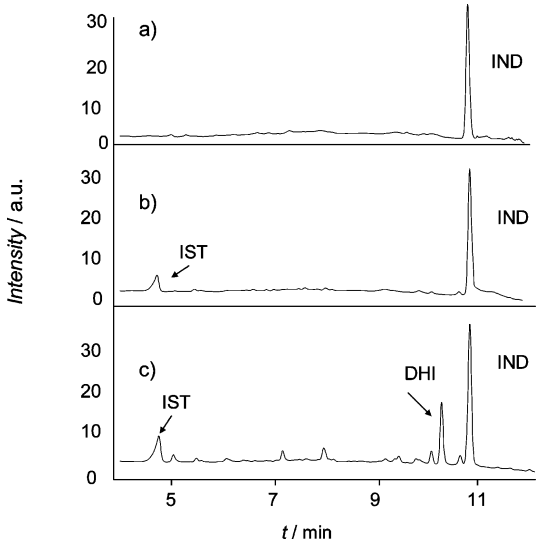

Figure 3. LC−DAD chromatograms of DMSO extracts of (a) IN_{160}, (b) IN@KA_{25}, and (c) IN@KA_{140}. IND = indigo, IST = isatin, and DHI = dehydroindigo.

dx.doi.org/10.1021/am402193u | ACS Appl. Mater. Interfaces 2013, 5, 8134−8145

can be seen for IN@KA_{140} in Figure 3. The majority components of the DMSO extracts were identified by means of their characteristic MS and ^{1}H and ^{13}C NMR signatures. Table 1 summarizes the pertinent identification data obtained from the DMSO extracts of the IN@MT_{150} sample. The ^{1}H and ^{13}C NMR spectra agreed well with those recorded for blanks of such compounds as well as with reported NMR data for indigo,[66] dehydroindigo,[57] and isatin.[67]

It can be deduced, however, that there is the possibility of promoting indigo oxidation as a result of an unexpected solvent-assisted reaction during the extraction/LC experiments. In fact, Dejoie et al.[68] have reported that even when protected inside a zeolite the indigo molecule can react with a chemical agent and be partly modified. To discard this possibility, blank experiments were performed by subjecting indigo powder to heating (IN_t specimens in the following) followed by subsequent extraction/LC analysis identical to those previously described for the IN@support specimens. As can be seen in Figure 3, the extract from indigo heated at 160 °C only shows the indigo peak with no traces of oxidation products. Remarkably, significant indigo oxidation and in particular oxidation yielding dehydroindigo are produced only upon dye attachment to the clay supports. This is consistent with the aforementioned data for indigo@$support_{25}$ and indigo@$support_t$ (T > 100 °C) specimens, which show that for all inorganic supports in this study dehydroindigo appears only in specimens heated above 100−120 °C. As far as the extraction and other processes performed at room temperature, if the indigo to dehydroindigo oxidation was the result of a reaction with the solvent, then this would occur also for the unheated specimens.

The LC data permits the verification of the important differences in the capability for dye attachment that exist between the studied inorganic supports. Figure 4 shows the

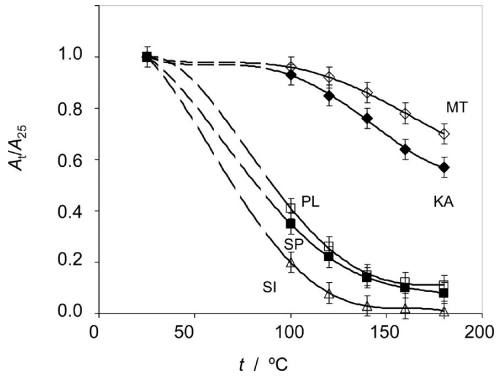

Figure 4. Variation of the total area of the chromatographic peaks in the DMSO extracts from IN@$support_t$ specimens relative to the total area in the extract from the corresponding IN@$support_{25}$ specimen with the temperature of the thermal treatment used to prepare such specimens.

variation of the total area of the chromatographic peaks (recorded as the sum of the peak areas in chromatograms such as in Figure 3) in the DMSO extracts from IN@$support_t$ (100 °C < T < 180 °C) specimens normalized with respect to the total area of the extracts from the corresponding IN@$support_{25}$, A_t/A_{25}. As can be seen in Figure 4, laminar clays display a slight decrease in the A_t/A_{25} ratio with the increase in the temperature of the thermal treatment used in the preparation of the specimens. This decrease can be attributed to the retention of some amount of indigo attached to the clay during the extraction experiments as well as the differences in the chromatographic coefficient of response (peak area/concentration) of indigo and the other dyes present in the extract. Remarkably, channeled clays and the MFI zeolite displayed a sharp decrease in the A_t/A_{25} ratio, denoting that in these heated IN@$support_t$ specimens significant amounts of the dye become firmly attached to the inorganic host (i.e., a low proportion of indigo and its oxidized forms is extractable). These results are consistent with the photographic images of the supernatant extract and the material submitted to extraction in Figure 1, which are illustrative of the aforementioned nontrapping effect existing in laminar clays. Thus, the supernatant DMSO solution concentrates almost quantitatively the dye mixture, whereas the remaining clay material becomes colorless.

Figure 5 permits the comparison of the area of the chromatographic peaks determined in the extracts from the

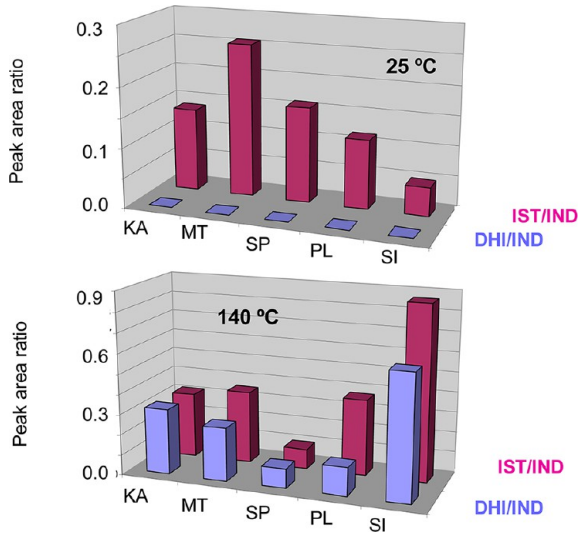

Figure 5. Comparison of the area of the chromatographic peaks (isatin/indigo and dehydroindigo/indigo ratios) determined in extracts from IN@KA_{25}, IN@MT_{25}, IN@SP_{25}, IN@PL_{25}, and IN@SI_{25} (top) as well as IN@KA_{140}, IN@MT_{140}, IN@SP_{140}, IN@PL_{140}, and IN@SI_{140} (lower) specimens using LC−DAD. IND = indigo, IST = isatin, and DHI = dehydroindigo.

IN@support specimens prepared at 25 °C and treated at 140 °C. Such data can be summarized as follows: (i) isatin is the unique oxidized form of indigo accompanying this dye in the extracts from all IN@$support_{25}$ samples, (ii) the (apparent, as determined from peak area ratios) isatin/indigo ratio of IN@$support_{25}$ specimens is larger for laminar clays than for channeled clays and is particularly low for IN@SI_{25}, (iii) the isatin/indigo ratio increases notably with the temperature of the thermal treatment, with the increase being particularly pronounced for silicalite, (iv) dehydroindigo appears as a significant component in all specimens treated above 100−120 °C, with the dehydroindigo/indigo ratio increasing significantly with the increase in the temperature for all IN@$support_t$ specimens, and (v) the dehydroindigo/isatin ratio increases significantly with the increase in the temperature in all cases so that dehydroindigo becomes the predominating oxidized form above 160 °C. These features can in principle be explained by considering that dehydroindigo and isatin are products of

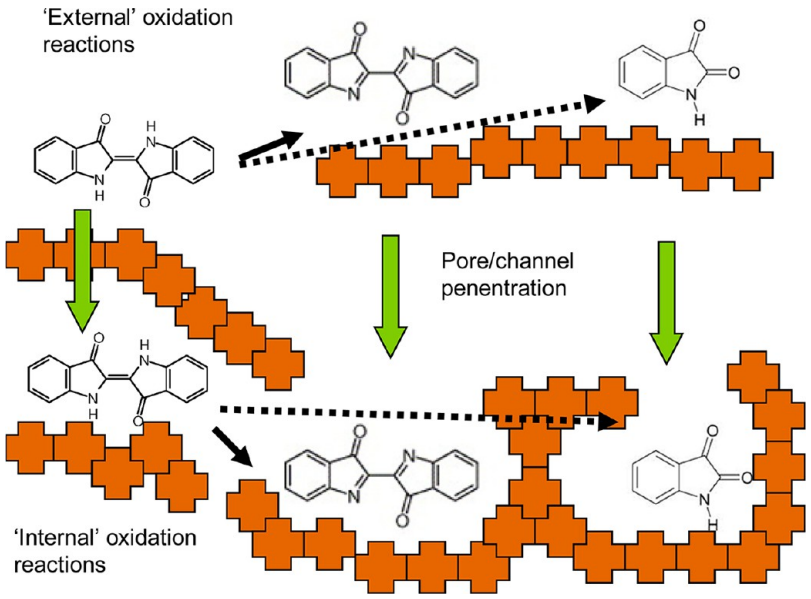

Figure 6. Scheme for the processes involved in the chemical oxidation of indigo to dehydroindigo and isatin in channeled supports.

support-assisted aerobic oxidations of indigo. These reactions can be represented as

$$\{C_{16}H_{10}O_2N_2\} + (1/2)O_2(g) \rightarrow \{C_{16}H_8O_2N_2\} + H_2O(g) \quad (1)$$

$$\{C_{16}H_{10}O_2N_2\} + O_2(g) \rightarrow 2\{C_8H_5O_2N\} \quad (2)$$

where { } denotes clay-associated species. From an exclusively thermodynamic point of view, the formation of dehydroindigo from indigo will be favored relative to the indigo to isatin oxidation by water abstraction at temperatures above 100 °C. Both reactions are endothermic, but one can expect a positive variation of entropy for the former so that the spontaneity of the process will be favored by temperature increase and the later would proceed with an entropy decrease so that temperature increase does not enhance spontaneity. This would justify that isatin was relatively abundant in the extracts from IN@support$_{25}$ specimens, whereas dehydroindigo was the predominating oxidized form in Maya Blue-type materials heated above 160 °C. The role of the inorganic supports, however, would be to act catalytically on the oxidation reactions. This situation, however, is additionally complicated by the possibility of the penetration of dye molecules into the pore/channel system of the MFI zeolite and the channeled clays. Tentatively, our LC data suggest that in these cases both reactions 1 and 2 can occur for indigo externally associated to the support and for indigo molecules penetrating more or less deeply in the pore/channel system of the support. Accordingly, there is a complex situation where the oxidation reactions occurring in the external surface compete with those occurring in the channels/pore that are in turn mediated by the diffusive penetration process itself, which is in principle a picture consistent with the prior kinetic study of IN@PL specimens.[59] Figure 6 shows a pictorial scheme for the above processes occurring in a channeled support. The data in Figures 4 and 5 clearly show that channeled clays (palygorskite and sepiolite) appear to be less efficient in promoting external indigo oxidation than are laminar clays (kaolinite and montmorillonite), whereas the MFI zeolite is particularly effective for promoting the oxidation of indigo to dehydroindigo and isatin. The specific catalytic sites and surface area as well as the size and geometry of the pore/channel system of the support should be balanced to interpret such differences, but it is obvious that further research is needed to properly elucidate such matters.

III.3. Solid-State Electrochemistry. The voltammetric response of the different IN@support species attached to graphite electrodes in contact with aqueous acetate buffer was studied by means of square wave voltammetry. All nonheated IN@support systems display a quite similar response, which is close to that of microcrystalline indigo, consisting of two intense peaks at +0.40 (I) and −0.34 V versus SCE (II) that are attributable to the proton-assisted solid-state oxidation of indigo to dehydroindigo and reduction of indigo to leucoindigo, as previously studied in detail.[44−49] The corresponding square wave voltammograms at a relatively high frequency for IN@MT$_{25}$ and IN@SI$_{25}$ are shown in Figure 7. Under these experimental conditions, the voltammetric response is representative of the composition of the external regions of the support crystals and, in agreement with previous results,[48,49] all materials present a similar voltammetric behavior. In contrast, thermally treated specimens produce additional peaks attributable to dye-localized processes. Such additional peaks differ from one clay to another, as can be seen in Figure 7 for IN@MT$_{150}$ and IN@SI$_{150}$. At low frequencies (i.e., at longer experimentation times), the voltammogram is representative of the advance of the diffusion layer into progressively deep regions in the clay crystals. The intensity of the indigo peaks then considerably decreases, and peak splitting appears for specimens heated above 100 °C. In particular, all unheated IN@support$_{25}$ specimens yield a unique peak (I), whereas for thermally treated specimens this peak is accompanied of additional anodic signals at +0.59 and +0.26 V, which is a behavior common to all supports (Supporting Information). This behavior can be interpreted as being indicative of the coexistence of different organic components[69,70] and/or differently attached to the clay support,[48,49] forming the so-called topological redox isomers, which is a feature introduced in zeolite electrochemistry.[50,71]

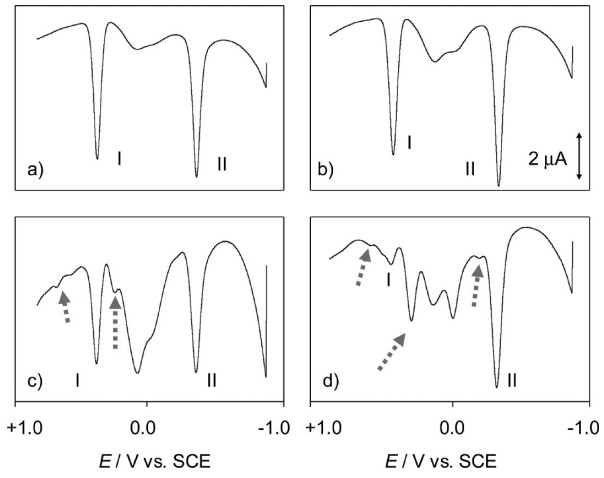

Figure 7. Square wave voltammograms of PIGEs modified with (a) IN@MT_{25}, (b) IN@SI_{25}, (c) IN@MT_{150}, and (d) IN@SI_{150} immersed into 0.25 M HAc/NaAc, pH 4.75. The potential scan was initiated at −0.85 V in the positive direction, with a potential step increment of 4 mV, a square wave amplitude of 25 mV, and a frequency of 50 Hz.

CA experiments confirmed the appearance of significant differences in the electrochemical behavior of laminar and porous/channeled materials. Figure 8a compares the CAs of the IN@KA_{140} and IN@SP_{140} specimens attached to graphite electrodes in contact with acetate buffer upon applying a potential of −0.35 V at which the proton-assisted reduction of indigo to leucoindigo occurs under diffusion-controlled conditions.[44−49] In these circumstances, the theoretical model developed by Lovric, Oldham, Scholz, and co-workers[72−75] on the electrochemistry of ion-insertion solids can be applied. On the basis of such a model, the charge passed at a time t can be taken as representative of the total number of electroactive molecules reached by the advance of the diffusion layer through the crystal during this time. The length of the diffusion layer advance can be estimated as $(Dt)^{1/2}$, with D being the effective diffusion coefficient associated with the coupled proton plus electron transfer in the solid material. At short times, the current/time response will be representative of the composition of the more external layers of the crystals, whereas the composition of deeper regions will determine the electrochemical response at longer times. In agreement with previously reported data,[48,49] all indigo@$support_{25}$ specimens provided monotonically decaying current/time curves, which is a feature that also occurrs for the thermally treated specimens prepared from laminar clays (kaolinite and montmorillonite) as well as for MFI zeolite. In contrast, CAs of heated channeled clays (palygorskite and sepiolite) provided current/time curves with an initial current increase followed by a slow decay, as can be seen in Figure 8. These CA curves can be described as being a result of the different in depth distribution of the electroactive guest dye in the grains of the clay host. Using the formalism previously reported[48] and taking $D = 1 \times 10^{-11}$ cm^2/s,[49] one can estimate the ratio between the concentration at a given depth, c, and the maximum dye concentration, c_{max}. Figure 8b shows the c/c_{max} versus depth (x) plots for the IN@KA_{140} and IN@SI_{140} specimens. The former is representative of the distribution of indigo molecules in kaolinite and montmorillonite specimens at all temperatures as well as in the sepiolite, silicalite, and palygorskite unheated specimens. The second is representative of the thermally treated specimens prepared from such porous/channeled supports. The in depth variation of the dehydroindigo/indigo ratio can also be estimated from chronoamperometric[48,49] and square wave voltammetric[76] data.

The above results were in agreement with EIS data where consistent differences were again obtained between the laminar clays and porous/channeled supports. Figure 9 compares the Nyquist and Bode plots of the impedance spectra of IN@KA_{25}

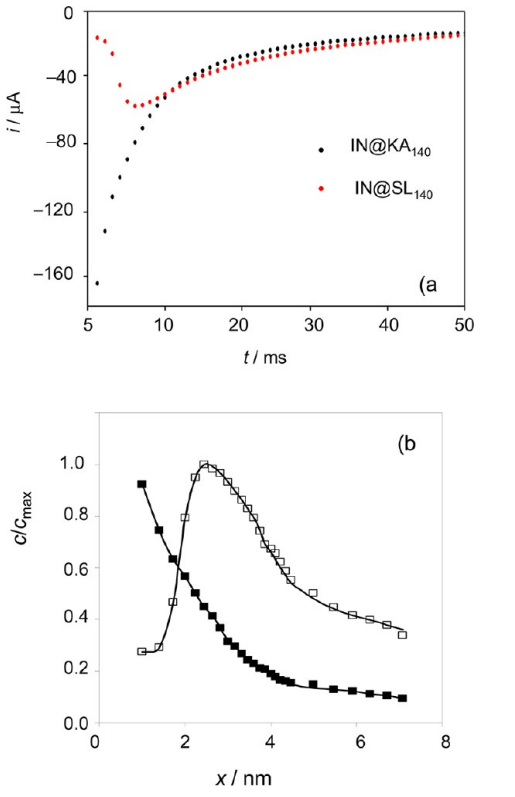

Figure 8. CAs of (a) IN@KA_{140} (black) and IN@SP_{140} (red) attached to paraffin-impregnated graphite electrodes in contact with 0.25 M HAc/NaAc, pH 4.75, with an applied potential of −0.35 V and plots of (b) c/c_{max} vs x for IN@KA_{140} (solid squares) and IN@SP_{140} (squares) estimated from the above CAs taking $D = 1 \times 10^{-11}$ cm^2/s.

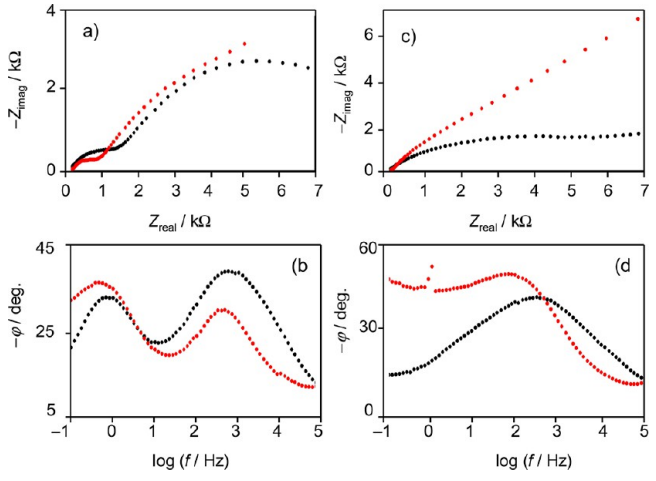

Figure 9. Nyquist (a,b) and Bode (c,d) plots for EIS spectra of IN@KA_{25} (black points) and IN@KA_{140} (red points) specimens attached to graphite electrodes in contact with a 2.5 mM $K_4Fe(CN)_6$ + 2.5 mM $K_3Fe(CN)_6$ solution in 0.25 M HAc/NaAc, pH 4.75, with applied potentials of (a,c) +0.25 V and (b,d) +0.45 V.

dx.doi.org/10.1021/am402193u | ACS Appl. Mater. Interfaces 2013, 5, 8134−8145

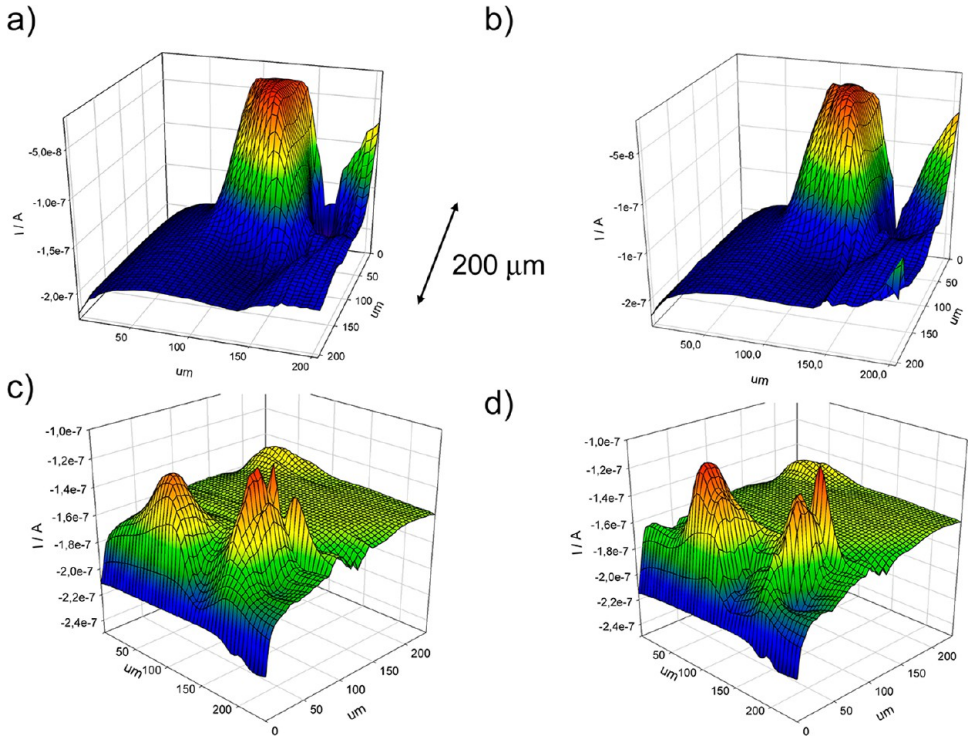

Figure 10. SECM topographic images of deposits of (a,b) IN@PL_{140} and (c,d) IN@PL_{25} onto a graphite plate in contact with a 5.0 mM $K_4Fe(CN)_6$ solution in 0.25 M HAc/NaAc, pH 4.75. (a,c) E_T = +0.35 V and E_S = 0.00 V and (b,d) E_T = +0.35 V and E_S = +0.55 V.

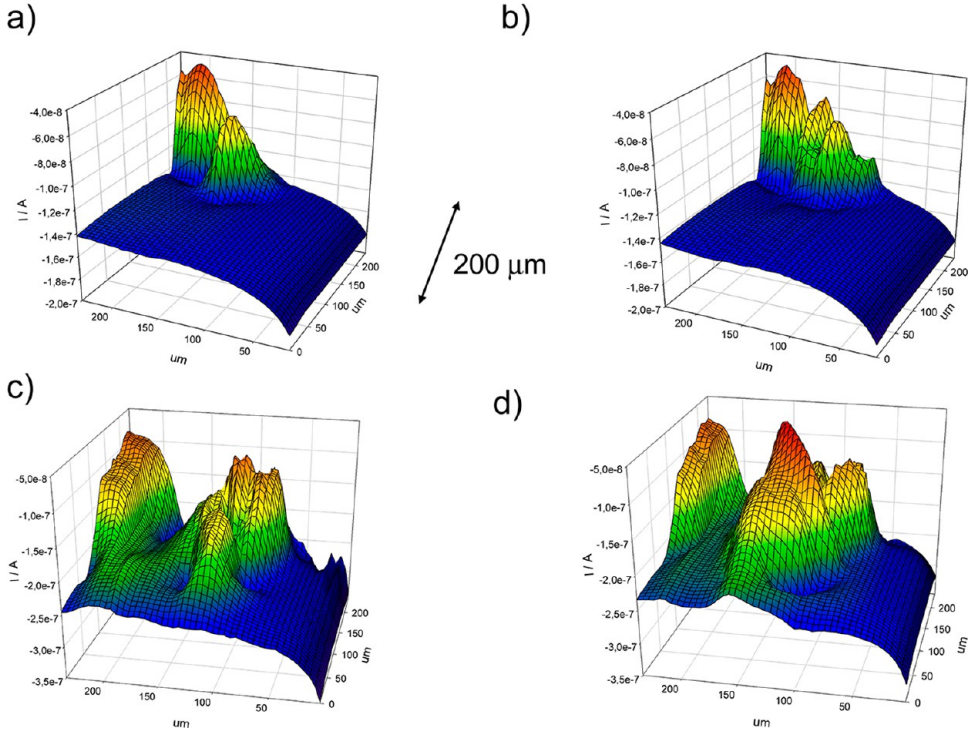

Figure 11. SECM topographic images of deposits of (a,b) IN@KA_{25} and (c,d) IN@KA_{140} onto a graphite plate in contact with a 5.0 mM $K_4Fe(CN)_6$ solution in 0.25 M HAc/NaAc, pH 4.75. (a,c) E_T = +0.35 V and E_S = 0.00 V and (b,d) E_T = +0.35 V and E_S = +0.55 V.

and IN@KA_{140} attached to graphite electrodes in contact with a $Fe(CN)_6^{3-}/Fe(CN)_6^{4-}$ solution in aqueous acetate buffer. Applying a bias potential above +0.25 V, the EIS spectra reflects the response of the modified electrode to the electrochemical oxidation of hexacyanoferrate(II) ion. When this potential is not high enough to promote the oxidation of indigo to dehydroindigo, both the unheated and heated materials yield essentially identical Nyquist and Bode plots (Figure 8a,b). The former consists of two successive capacitive loops, whereas two well-defined maxima at intermediate and low frequencies appear in the Bode plots. When the bias potential is sufficiently large enough to promote the additional oxidation of indigo to

dx.doi.org/10.1021/am402193u | ACS Appl. Mater. Interfaces 2013, 5, 8134−8145

dehydroindigo, significant differences appear between such specimens, as can be seen in Figure 9c,d. Here, the Nyquist plots consist of a capacitive depressed semicircle at high frequencies accompanied by a linear branch at low freqeuncies. This response can be fitted to a Randless−Ershler circuit consisting of a series arrangement of the solution resistance with a parallel arrangement of a double-layer capacitor and a series combination of charge-transfer resistance plus Warburg impedance. This last element reflects the diffusing properties of hexacyanoferrate(II) ions approaching the electrode surface to be oxidized so that the observed profile in Figure 9a,b fits with the theoretical for transmissive reflective diffusion conditions, whereas the Nyquist plots in Figure 9c,d corresponds to diffusion under semiinfinite boundary conditions.[77,78]

The behavior in Figure 9a,b was common for all IN@support$_t$ specimens and denotes that (in conditions where no indigo-localized redox processes occur) the EIS response is essentially independent of the dye composition. However, in all cases, when the EIS experiment is performed under conditions where the oxidation of $Fe(CN)_6^{4-}$ to $Fe(CN)_6^{3-}$ is accompanied by the electrochemical oxidation of indigo to dehydroindigo (Figure 9c,d), there are significant differences in the spectra of IN@support$_{25}$ specimens and those of specimens treated at temperatures above 100 °C. As can be seen in Figure 9c,d for IN@KA$_{25}$ and IN@KA$_{140}$, such differences are particularly significant in the low-frequency region. This feature is in principle attributable to two combined factors: (i) the contribution of the additional Faradaic process consisting of indigo oxidation to dehydroindigo to charge-transfer resistance and (ii) diffusive effects (proton diffusion in the clay and in the solution phase) resulting in increasing Warburg impedance.

The effect of the different dye compositions can in principle also be related with changes in the SECM topographies on the basis of generation/collection[53] and redox competition[79−81] methods. Again, differences were found between unheated and thermally treated specimens of laminar clays and porous/channeled supports. As can be seen in Figures 10 and 11, topographic SECM images of a deposit of IN@PL$_{25}$ on a graphite plate in contact with a $K_4Fe(CN)_6$ solution in acetate buffer show particulate aggregates on graphite laminae. If the tip is maintained at a potential E_T sufficiently high to oxidize $Fe(CN)_6^{4-}$ ions to $Fe(CN)_6^{3-}$ ones (+0.35 V) and the substrate is maintained at a potential E_S where the above process does not occur (Figure 10a), then the tip current reflects the local variations in the conductivity of the substrate where no Faradaic reactions take place. Thus, the topographic image shows spaced peaked features corresponding to palygorskite particles on the graphite substrate. If the substrate is held at a potential of +0.55 V and the tip is maintained at +0.35 V, then both the oxidation of clay-associated indigo to dehydroindigo and the oxidation of $Fe(CN)_6^{4-}$ to $Fe(CN)_6^{3-}$ at the bare graphite can occur. In the case of phyllosilicate clays and MFI zeolite, the heated specimens show essentially no change in the particle topography when E_S is passed from 0.00 to +0.55 V, as can be seen by comparing Figure 10 panels a and b for IN@PL$_{140}$. In such specimens, this result can be rationalized by considering that dye molecules are predominantly internal and that a significant amount of dehydroindigo exists. On the contrary, for the nonheated specimens of palygorskite, sepiolite, and silicalite, when E_S was changed from 0.00 to +0.55 V, there was a significant topographic change, as can be seen by comparing Figure 10 panels c and d, corresponding to IN@PL$_{25}$. First of all, it should be noted that topographic changes occur in the region of the clay grains in contact with the graphite/particle/electrolyte junction, as was expected on the basis of the previously mentioned theoretical modeling.[72−75] In the case of IN@PL$_{25}$, as in all nonheated specimens, topographic changes can be associated with the oxidation of indigo to dehydroindigo occurring when E_S > 0.40 V. In those samples, indigo remains externally attached to the clay, and only a minimal fraction is oxidized mainly to isatin so that important electrochemical oxidation occurs at these potentials.

In the case of laminar clays, the topographic changes were observed in both unheated and heated specimens when the substrate potential was moved from 0.00 to +0.55 V, as shown in Figure 11 for IN@K$_{25}$ and IN@KA$_{140}$. The topographic change was larger for the unheated material than for those thermally treated. These features can be attributed to the availability of indigo to undergo electrochemical oxidation, which is consistent with the idea that indigo remains externally attached to the inorganic support in laminar clays. In the case of porous clays where a repository of internal indigo is stored in the clay crystals, the advance of the indigo oxidation process could be reflected in the previously indicated more drastic variations in the SECM response.

It is pertinent to note that SECM experiments involve a relatively long time scale (5−30 min) so that under the aforementioned diffusion-controlled conditions there is place for a significant progress of the electrochemical indigo oxidation when E_S is high enough to promote such process. Also, it should be noted that the observed profiles in Figures 10 and 11 correspond to electrochemical topographies that are representative of the local redox reactivity of the substrate electrode and the materials deposited on it.

III.4. On 'Genuine' Maya Blue-Type Materials. The reported data indicate unambiguously that dehydroindigo, isatin, and other minority organic compounds accompany indigo in Maya Blue-type materials prepared by means of the dry (crushing indigo with the powdered clay and heating at 100 − 180 °C) method using indigo loadings of ca. 1 wt %. In laminar aluminosilicate clays, the organic components remain externally adsorbed on the surface of the clay crystals, and the extensive removal of such components is obtained via conventional extraction with organic solvents. In the case of porous/channeled supports, a significant amount of the dye mixture became attached to the clay support and is not removed in extraction experiments.

Remarkably, the oxidation processes appear to require the interaction of the dye with the clay support, as denoted by blank experiments in unsupported indigo. Consistently, a recent study from Sousa et al.[82] showed that the degradation of indigo to isatin under light excitation in the presence and absence of molecular oxygen in solution (homogeneous) and gels (heterogeneous) media was considerably difficult. All of these features suggest that the inorganic support plays a significant catalytic role on the oxidation of indigo to dehydroindigo and isatin.

The dye/clay composition in archeological Maya Blue samples can be determined using voltammograms such as in Figure 6 by measuring the peak current for the indigo/dehydroindigo peaks at +0.40 V (or the indigo/leucoindigo peak at −0.34 V), i_{pdye}, and the height of background signals appearing between 0.0 and +0.25 V, i_{back}. In agreement with the literature for carbon electrodes,[83,84] these last signals can be attributed to oxygen-based functionalities associated with the

scratching of the graphite surface. Figure 12 shows a calibration curve for the synthetic IN@PL$_{150}$ specimens. Under our

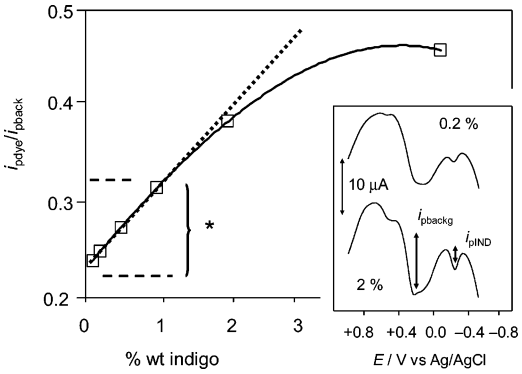

Figure 12. Variation of the i_{pdye}/i_{pback} ratio on the indigo loading for synthetic Maya Blue-type specimens prepared from indigo and palygorskite and treated at 150 °C for 24 h. The inset corresponds to the square wave voltammograms for 0.2 and 2 wt % indigo specimens in contact with aqueous acetate buffer in conditions such as those in Figure 5.

experimental conditions, the i_{pdye}/i_{back} ratio varies linearly with the weight percentage of indigo for dye percentages between 0.1 and ca. 2%, deviating from linearity for larger indigo loadings. Insertion of the i_{pdye}/i_{back} ratios measured for genuine Maya Blue samples[44−47] into the above calibration data permits the estimation of the indigo loading in genuine Maya Blue specimens, which range between 0.2 and 1.5 wt % of indigo. Obviously, this estimate should be taken with caution because in archeological samples palygorskite was accompanied by $CaCO_3$ and other components varying from one archeological site to another.[45,46]

Extraction experiments suggest that in materials prepared from higher indigo loadings[23,24,28,29,37] the majority of the dye remains as aggregated indigo microcrystals[29] so that the spectral features of organic compounds other than indigo become obscured by those of the majority dye. This means that the composition and spectral properties of these materials are separated from those of historical Maya Blue, which is constrained to dye loadings of ca. 1 wt %.[28]

The data presented here, in agreement with our previous reports,[44−49] suggest that an inherent property of historical Maya Blue and hence genuine Maya Blue-type materials is the coexistence of different organic dyes. This multicomponent nature would be essential to explain the peculiar hue variability of Maya Blue: the color of Maya Blue would result from mainly the batochromic shift of the indigo absorption bands resulting from the dye attachment to the clay combined with the spectral features of clay-associated dehydroindigo and the variable dehydroindigo/indigo ratio (controllable by varying the temperature and duration of the thermal treatment as well as the crushing process), which would determine the variations in the hue of the material.[44−49] Recent archeological discoveries on Maya yellow[69] and Maya green[70] organic−inorganic hybrid materials can be considered to be consistent with the existence of a Maya Blue chemistry exploiting the natural components available to the ancient Mayan people.

IV. CONCLUSIONS

Synthetic specimens prepared upon indigo attachment to kaolinite, montmorillonite, sepiolite, silicalite, and palygorskite supports exhibited a characteristic blue-greenish hue after application of thermal treatments between 100 and 180 °C. Extraction with DMSO provided evidence for the presence of significant amounts of dehydroindigo and isatin accompanying indigo in the extracts, which were identified by their characteristic spectral, NMR, and MS signatures. Significant differences exist between the specimens prepared with laminar clays and those from microporous clays. In the case of the former, the dye is almost quantitatively removed from the clay support in both the thermally treated and unheated specimens, which is in agreement with the idea that dye molecules are externally bound to the clay crystals. However, samples prepared from porous/channeled supports retained significant amount of the dye after equivalent extraction experiments. The retained dye loading was clearly larger for the thermally treated specimens than for unheated ones, denoting the existence of the strong internal attachment of the dyes to the aluminosilicate support in such cases.

Electrochemical (SWV, CA, EIS, and SECM) data provided evidence for the ubiquitous presence of dehydroindigo accompanying indigo in the solid materials and permitted the estimation of the indigo loading in archeological Maya Blue to be in the 0.2−1.5 wt % range. These results confirm previous reports introducing other indigo organic components, dehydroindigo in particular, into the Maya Blue scenario as well as their concomitant importance for interpreting the peculiar hue variability of the pigment and for describing Maya Blue as a polyfunctional inorganic−organic hybrid material.

■ ASSOCIATED CONTENT

Supporting Information

Experimental details, TEM images of IN@SI and IN@MT specimens, and additional voltammetric data. This material is available free of charge via the Internet at http://pubs.acs.org.

■ AUTHOR INFORMATION

Corresponding Author

*E-mail: antonio.domenech@uv.es. Tel: +34-963544533.

Notes

The authors declare no competing financial interest.

■ ACKNOWLEDGMENTS

Financial support is gratefully acknowledged from the MICINN, projects CTQ2011-28079-CO3-01 and 02, which are also supported with ERDF funds.

■ REFERENCES

(1) Sánchez, C.; Ribot, F. *New J. Chem.* **1994**, *18*, 1007−1047.
(2) Sánchez, C.; Julian, B.; Belleville, P.; Popall, M. *J. Mater. Chem.* **2005**, *14*, 3559−3592.
(3) Calzaferri, G.; Huber, S.; Maas, H.; Minkowski, C. *Angew. Chem., Int. Ed.* **2003**, *42*, 3732−3758.
(4) Romero, P.; Sánchez, C. *New J. Chem.* **2005**, *29*, 57−58.
(5) Morris, E. H. In *The Temple of the Warriors at Chichen Itza, Yucatan.* Morris, E. H., Charlot, J., Morris, A. A., Eds.; Carnegie Institution: Washington, 1931; p 356.
(6) Sheppard, A. O. *Am. Antiq.* **1962**, *27*, 565−566.
(7) Kleber, R.; Masschelein-Kleiner, R.; Thissen, J. *Stud. Conserv.* **1967**, *12*, 41−56.
(8) José-Yacamán, M.; Rendón, L.; Arenas, J.; Serra-Puche, M. C. *Science* **1996**, *273*, 223−225.
(9) Fernández, M. E.; Ascencio, J. A.; Mendoza-Anaya, D.; Rodríguez-Lugo, V.; José-Yacamán, M. *J. Mater. Sci.* **1999**, *34*, 5243−5255.

(10) Polette, L. A.; Meitzner, G.; José-Yacamán, M.; Chianelli, R. R. *Microchem. J.* **2002**, *71*, 167−174.
(11) Chiari, G.; Giustetto, R.; Ricchiardi, G. *Eur. J. Mineral.* **2003**, *15*, 21−33.
(12) Hubbard, B.; Kuang, W.; Moser, A.; Facey, G. A.; Detellier, C. *Clays Clay Miner.* **2003**, *51*, 318−326.
(13) Fois, E.; Gamba, A.; Tilocca, A. *Microporous Mesoporous Mater.* **2003**, *57*, 263−272.
(14) Reinen, D.; Köhl, P.; Müller, C. *Z. Anorg. Allg. Chem.* **2004**, *630*, 97−103.
(15) Sánchez del Río, M.; Martinetto, P.; Somogyi, A.; Reyes-Valerio, C.; Dooryhée, E.; Peltier, N.; Alianelli, L.; Moignard, B.; Pichon, L.; Calligaro, T.; Dran, J.-C. *Spectrochim. Acta, Part B* **2004**, *59*, 1619−1625.
(16) Sánchez del Rio, M.; Sodo, A.; Eeckhout, S. G.; Neisius, T.; Martinetto, P.; Dooryhee, E.; Reyes-Valerio, C. *Nucl. Instrum. Methods Phys. Res., Sect. B.* **2005**, *238*, 50−54.
(17) Giustetto, R.; Llabrés i Xamena, F. X.; Ricchiardi, G.; Bordiga, S.; Damin, A.; Gobetto, R.; Chierotti, M. R. *J. Phys. Chem. B* **2005**, *109*, 19360−19368.
(18) Chianelli, R. R.; Perez de la Rosa, M.; Meitzner, G.; Siadati, M.; Berhault, G.; Mehta, A. *J. Synchrotron Radiat.* **2005**, *12*, 129−134.
(19) Manciu, F. S.; Reza, L.; Polette, L. A.; Torres, B.; Chianelli, R. R. *J. Raman Spectrosc.* **2007**, *38*, 1193−1198.
(20) Polette-Niewold, L. A.; Manciu, F. S.; Torres, B.; Alvarado, M.; Chianelli, R. R. *J. Inorg. Biochem.* **2007**, *101*, 1958−1973.
(21) Chiari, G.; Giustetto, R.; Druzik, J.; Doehne, E.; Ricchiardi, G. *Appl. Phys. A: Mater. Sci. Process.* **2008**, *90*, 3−7.
(22) Tilocca, A.; Fois, E. *J. Phys. Chem. C* **2009**, *113*, 8683−8687.
(23) Sánchez del Río, M.; Boccaleri, E.; Milanesio, M.; Croce, G.; van Beek, W.; Tsiantos, C.; Chyssikos, G. D.; Gionis, V.; Kacandes, G. H.; Suárez, M.; García-Romero, E. *J. Mater. Sci.* **2009**, *44*, 5524−5536.
(24) Tsiantos, C.; Tsampodimou, M.; Kacandes, G. H.; Sánchez del Río, M.; Gionis, V.; Chryssikos, G. D. *J. Mater. Sci.* **2012**, *47*, 3415−3428.
(25) Reyes-Valerio, C. *De Bonampak al Templo Mayor: El Azul Maya en Mesoamérica*; Siglo XXI: México, D.F., 1993.
(26) Van Olphen, H. *Science* **1967**, *154*, 645−646.
(27) Lima, E.; Guzmán, A.; Vera, M.; Rivera, J. L.; Fraissard, J. *J. Phys. Chem. C* **2012**, *116*, 4556−4563.
(28) Mondelli, C.; Sánchez del Río, M.; González, M. A.; Magazzú, A.; Cavalleri, C.; Suárez, M.; García-Romero, E.; Romano, P. *J. Phys.: Conf. Ser.* **2012**, *340*, 1−6.
(29) Dejoie, C.; Martinetto, P.; Dooryhée, E.; Brown, R.; Blanc, S.; Bordat, P.; Strobel, P.; Odier, P.; Porcher, F.; Sanchez del Rio, M.; Van Eslande, E.; Walter, P.; Anne, M. *Mater. Res. Soc. Symp. Proc.* **2011**, *1319*, 103−115.
(30) Ovarlez, S.; Giulieri, F.; Chaze, A.-M.; Delamare, F.; Raya, J.; Hirschinger, J. *Chem.−Eur. J.* **2010**, *15*, 11326−11332.
(31) Giustetto, R.; Seenivasan, K.; Bonino, F.; Ricchiardi, G.; Bordiga, S.; Chierotti, M. R.; Gobetto, R. *J. Phys. Chem. C* **2011**, *115*, 16764−16776.
(32) Volle, N.; Challier, L.; Burr, A.; Giulieri, F.; Pagnotta, S.; Chaze, A.-M. *Compos. Sci. Technol.* **2011**, *71*, 1685−1691.
(33) Giustetto, R.; Levy, D.; Wahyudi, O.; Ricchiardi, G.; Vitillo, J. G. *Eur. J. Mineral.* **2011**, *23*, 449−466.
(34) Ovarlez, S.; Giulieri, F.; Delamare, F.; Sbirrazzuoli, N.; Chaze, A.-M. *Microporous Mesoporous Mater.* **2011**, *142*, 371−380.
(35) Giustetto, R.; Wahyudi, O.; Corazzari, I.; Turci, F. *Appl. Clay Sci.* **2011**, *52*, 41−50.
(36) Giulieri, F.; Ovarlez, S.; Chaze, A.-M. *Int. J. Nanotechnol.* **2012**, *9*, 605−617.
(37) Dejoie, C.; Martinetto, P.; Dooryhée, E.; Strobel, P.; Blanca, S.; Bordat, P.; Brown, R.; Porcher, F.; Sanchez del Rio, M.; Anne, M. *ACS Appl. Mater. Interfaces* **2010**, *2*, 2308−2316.
(38) Kowalak, S.; Zywert, A. *Clay Miner.* **2011**, *46*, 197−204.
(39) Giustetto, R.; Wahyudi, O. *Microporous Mesoporous Mater.* **2011**, *142*, 221−235.
(40) Giustetto, R.; Seenivasan, K.; Pellerej, D.; Ricchiardi, G.; Bordiga, S. *Microporous Mesoporous Mater.* **2012**, *155*, 167−176.
(41) Scholz, F.; Meyer, B. *Electroanalytical Chemistry: A Series of Advances*; CRC Press: Boca Raton, FL, 1998; Vol. *20*, pp 1−86.
(42) Scholz, F.; Schröder, U.; Gulaboski, R. *Electrochemistry of Immobilized Particles and Droplets*; Springer: Berlin, 2005.
(43) Doménech, A.; Labuda, J.; Scholz, F. *Pure Appl. Chem.* **2013**, *85*, 609−632.
(44) Doménech, A.; Doménech, M. T.; Vázquez, M. L. *J. Phys. Chem. B* **2006**, *110*, 6027−6039.
(45) Doménech, A.; Doménech, M. T.; Vázquez, M. L. *J. Phys. Chem. C* **2007**, *111*, 4585−4595.
(46) Doménech, A.; Doménech, M. T.; Vázquez, M. L. *Anal. Chem.* **2007**, *79*, 2812−2821.
(47) Doménech, A.; Doménech, M. T.; Vázquez, M. L. *Archaeometry* **2009**, *51*, 1015−1034.
(48) Doménech, A.; Doménech, M. T.; Sánchez del Río, M.; Goberna, S.; Lima, E. *J. Phys. Chem. C* **2009**, *113*, 12118−12131.
(49) Doménech, A.; Doménech, M. T.; Sánchez del Río, M.; Vázquez, M. L. *J. Solid State Electrochem.* **2009**, *13*, 869−878.
(50) Doménech, A. *Electrochemistry of Porous Materials*; Taylor & Francis: Boca Raton, FL, 2010.
(51) Yasarawan, N.; van Duijneveldt, J. S. *Langmuir* **2008**, *24*, 7184−7192.
(52) Doménech, A.; Doménech, M. T.; Valle-Algarra, F. M.; Dómine, M. E.; Osete-Cortina, L. *J. Mater. Sci.* **2013**, *48*, 7171−7183.
(53) *Scanning Electrochemical Microscopy*; Bard, A. J., Mirkin, M. V., Eds.; Marcel Dekker: New York, 2001.
(54) Battistel, D.; Daniele, S.; Fratter, D. *Electrochim. Acta* **2012**, *78*, 557−562.
(55) Salamifar, S. E.; Mehrgardi, M. A.; Kazemi, S. H.; Mousavi, M. F. *Electrochim. Acta* **2010**, *56*, 896−904.
(56) Hein, M.; Phuong, N. T. B.; Michalik, D.; Görls, H.; Lalk, M.; Langer, P. *Tetrahedron Lett.* **2006**, *47*, 5741−5745.
(57) Rondao, R.; De Melo, J. S.; Bonifacio, B. D.; Melo, M. J. *J. Phys. Chem. A* **2010**, *114*, 1699−1708.
(58) Yang, Z.; Lin, Y. S. *Ind. Eng. Chem. Res.* **2000**, *39*, 4944−4948.
(59) Doménech, A.; Doménech, M. T.; Osete, L.; Montoya, N. *Microporous Mesoporous Mater.* **2013**, *166*, 123−130.
(60) Ma, C.; Eggleton, R. A. *Clays Clay Miner.* **1999**, *47*, 181−191.
(61) Klevtsov, D. P.; Logvinenko, V. A.; Zolotvskii, V. P.; Krivoruchko, O. P.; Buyanov, R. A. *J. Therm. Anal. Calorim.* **1988**, *33*, 531−535.
(62) Frost, R. L.; Vassallo, A. M. *Clays Clay Miner.* **1996**, *44*, 635−651.
(63) Mori, H.; Miyoshi, H.; Takeda, K.; Yoneyama, H.; Fujita, H.; Iwata, Y.; Osaka, Y.; Murata, Y. *J. Mater. Sci.* **1992**, *27*, 3197−3199.
(64) García-Romero, E.; Súarez-Barrios, M.; Santarén-Rome, J.; Álvarez-Berenguer, A. *Clays Clay Miner.* **2007**, *55*, 606−617.
(65) Elias, M.; Chartier, C.; Prevot, G.; Garay, H.; Vignaud, C. *Mater. Sci. Eng., B* **2006**, *127*, 70−80.
(66) Hoffman, R. C.; Zilber, R. C.; Hoffman, R. E. *Magn. Reson. Chem.* **2010**, *48*, 892−895.
(67) Laatsch, H.; Thomson, R. H.; Cox, P. J. *J. Chem. Soc., Perkin Trans.* **1984**, *2*, 1331−1339.
(68) Dejoie, C.; Martinetto, P.; Dooryhée, E.; Van Elslande, E.; Blanc, S.; Bordat, P.; Brown, R.; Porcher, F.; Michel, A. *Appl. Spectrosc.* **2010**, *64*, 1131−1138.
(69) Doménech, A.; Doménech, M. T.; Vázquez, M. L. *Angew. Chem., Int. Ed.* **2011**, *50*, 5741−5744.
(70) Doménech, A.; Doménech, M. T.; Vidal, C.; Vázquez, M. L. *Angew. Chem., Int. Ed.* **2012**, *51*, 700−703.
(71) Bessel, C. A.; Rolison, D. R. *J. Phys. Chem. B* **1997**, *101*, 1148−1157.
(72) Lovric, M.; Scholz, F. *J. Solid State Electrochem.* **1997**, *1*, 108−113.
(73) Lovric, M.; Scholz, F. *J. Solid State Electrochem.* **1999**, *3*, 172−175.
(74) Oldham, K. B. *J. Solid State Electrochem.* **1998**, *2*, 367−377.

(75) Schröder, U.; Oldham, K. B.; Myland, J. C.; Mahon, P. J.; Scholz, F. *J. Solid State Electrochem.* **2000**, *4*, 314−324.
(76) Doménech, A.; Martini, M.; De Carvalho, L. M.; Doménech, M. T. *J. Electroanal. Chem.* **2012**, *684*, 13−19.
(77) Dell'Era, A.; Pasquali, M. *J. Solid State Electrochem.* **2009**, *13*, 849−859.
(78) Kuang, F.; Zhang, D.; Li, Y.; Wan, Y.; Hou, B. *J. Solid State Electrochem.* **2009**, *13*, 385−390.
(79) Karnicka, K.; Eckhard, K.; Guschin, D. A.; Stoica, L.; Kulesza, P. J.; Schumann, W. *Electrochem. Commun.* **2007**, *9*, 1998−2002.
(80) Guadagnini, L.; Maljusch, A.; Chen, X.; Neugebauer, S.; Tonelli, D.; Schumann, W. *Electrochim. Acta* **2009**, *54*, 3753−3758.
(81) Santana, J. J.; González-Guzmán, J.; Fernández-Mérida, L.; González, S.; Souto, R. M. *Electrochim. Acta* **2010**, *55*, 4488−4494.
(82) Sousa, M. M.; Miquel, C.; Rodrigues, I.; Parola, A. J.; Pina, F.; Seixas de Melo, J. S.; Melo, M. J. *Photochem. Photobiol. Sci.* **2008**, *7*, 1353−1359.
(83) Barisci, J. N.; Wallace, G. G.; Baughman, R. H. *Electrochim. Acta* **2000**, *46*, 509−517.
(84) Barisci, J. N.; Wallace, G. G.; Baughman, R. H. *J. Electroanal. Chem.* **2000**, *488*, 92−98.